



HAL
open science

Generalized Integrator-Extended State Observer With Applications to Grid-Connected Converters in the Presence of Disturbances

Baoling Guo, Seddik Bacha, Mazen Alamir, Ahmad Hably, Cédric Boudinet

► **To cite this version:**

Baoling Guo, Seddik Bacha, Mazen Alamir, Ahmad Hably, Cédric Boudinet. Generalized Integrator-Extended State Observer With Applications to Grid-Connected Converters in the Presence of Disturbances. IEEE Transactions on Control Systems Technology, 2021, 29 (2), pp.744 - 755. 10.1109/TCST.2020.2981571 . hal-03016035v1

HAL Id: hal-03016035

<https://hal.science/hal-03016035v1>

Submitted on 20 Nov 2020 (v1), last revised 20 Jan 2022 (v2)

HAL is a multi-disciplinary open access archive for the deposit and dissemination of scientific research documents, whether they are published or not. The documents may come from teaching and research institutions in France or abroad, or from public or private research centers.

L'archive ouverte pluridisciplinaire **HAL**, est destinée au dépôt et à la diffusion de documents scientifiques de niveau recherche, publiés ou non, émanant des établissements d'enseignement et de recherche français ou étrangers, des laboratoires publics ou privés.

Generalized Integrator-Extended State Observer With Applications to Grid-Connected Converters in the Presence of Disturbances

Baoling Guo¹, Seddik Bacha¹, *Senior Member, IEEE*, Mazen Alamir, *Member, IEEE*, Ahmad Hably, *Member, IEEE*, and Cédric Boudinet

Abstract—Large-scale fast-varying sinusoidal disturbances (FVSDs) strongly impact the operation of Grid-connected Converters (GcCs). A conventional extended state observer (ESO) is not sufficiently capable to deal with these rapid disturbances. This critical weakness has limited ESO's applications to GcCs. Therefore, a generalized integrator-ESO (GI-ESO) is developed from ESO to address such issues. Knowing that grid common disturbances can be expressed as a phase, frequency, or magnitude disturbed sinusoidal signal, multi-GIs of selective resonant frequencies are, hence, applied into the disturbance estimation loop, which enables FVSD to be observed with relatively low bandwidth. Besides, a frequency-adaptive mechanism is introduced in order to mitigate the effects of frequency deviations. The proposed GI-ESO resolves the tradeoff between the observer's bandwidth and noise filtering. A case of the three-phase phase-locked loop control system of disturbed regimes is, in particular, studied to assess the performance of GI-ESO and the stability of the resulting controlled system. Theoretical analysis and experimental results have proven its effectiveness in applications to GcCs in the presence of various disturbances.

Index Terms—Extended state observer (ESO), fast-varying sinusoidal disturbances (FVSDs), frequency-adaptive mechanism, generalized integrator (GI), grid-connected converters (GcCs), phase-locked loop (PLL).

I. INTRODUCTION

DISTURBANCES and uncertainties present in the control systems require the design of robust controllers [1]–[5]. Thus, various robust approaches based on disturbance rejection have been proposed, such as unknown input observer [1], disturbance observer [2], and extended state observer (ESO) [3]–[5]. However, the performance of model-based observers and its resulting control systems are sensitive to

model parameters deviations [2]. ESO has been widely used as a partial-model-based observer, being less dependent on the knowledge of the system [3]–[8]. ESO is proposed in the frame of active disturbance rejection control (ADRC), which can also work independently with other controllers [6]. ESO has been originally proposed with a nonlinear structure [3], while the linear ESO has been broadly employed as it is easier to design and to implement for practitioners [4].

The performances of ADRC- or ESO-based controllers primarily depend upon the accuracy of the state and disturbances estimation [3]. Large efforts have been devoted to the tracking error convergence analysis of nonlinear or linear ESOs [9]–[12]. Guo and Zhao [9] and Yoo *et al.* [10] have, respectively, proven that ESO can achieve the asymptotic convergence for constant disturbances. In another work [11], it has been shown that the ESO estimation error remains bounded if the changing rate of time-varying uncertainties is bounded. Theoretically, the estimation precision of ESO for time-varying disturbances can be improved by increasing its bandwidth. However, the bandwidth is limited by the presence of sensor noises and dynamic uncertainties; otherwise, large high-frequency noises from the output side would be transferred to the control signal [13]. Many attempts have been made to deal with a class of time-varying disturbances in [14]–[18]. A proportional–integral–generalized (GPI) observer-based control approach has been discussed in [15] and [16], which is actually in line with the generalized ESO (GESO) presented in [14]. A spatial observer-based repetitive controller is then proposed for mechatronic systems in [17], which is developed from the GPI approach described in [15] and [16]. It has been proven that if the r th-order derivative of disturbance becomes zero, the asymptotic convergence for its state estimate can be achieved by employing the r th-order GESO or GPI in [14]–[16]. However, a sinusoid is a type of infinitely differentiable disturbances [14]. The performance of higher order ESO in tracking sinusoidal disturbances has been analyzed in [12]. It has been shown that a higher order GESO offers better estimation accuracy in comparison with a conventional ESO, provided that the observer bandwidth is chosen sufficiently larger than the frequency of the disturbance. Consequently, the higher order GESO or GPI can only ensure the precision of limitedly low-frequency sinusoidal disturbances. The GESO/GPI is not sufficiently capable to deal with very fast-varying sinusoidal disturbances (FVSDs), such as harmonics-related disturbances that are multiples of grid

Manuscript received January 17, 2020; accepted March 12, 2020. Manuscript received in final form March 13, 2020. This work is supported and financed by (Projet Structurant des Pôles de Compétitivité) PSPC Innov'hydro. This project brings together General Electric (GE) Renewable Energy, eDF (Electricité de France), Grenoble INP, and other key players in the hydroelectric sector, in France. Recommended by Associate Editor G. Pin. (Corresponding author: Baoling Guo.)

Baoling Guo, Seddik Bacha, and Cédric Boudinet are with the Grenoble Electrical Engineering Laboratory (G2Elab), CNRS, Institute of Engineering (Grenoble INP), Université Grenoble Alpes, F-38000 Grenoble, France (email: baoling.guo@g2elab.grenoble-inp.fr; seddik.bacha@g2elab.grenoble-inp.fr; cedric.boudinet@g2elab.grenoble-inp.fr).

Mazen Alamir and Ahmad Hably are with the GIPSA-Lab, CNRS, Institute of Engineering (Grenoble INP), Université Grenoble Alpes, F-38400 Saint Martin D'Hères, France (e-mail: mazen.alamir@gipsa-lab.grenoble-inp.fr; ahmad.hably@gipsa-lab.grenoble-inp.fr).

Color versions of one or more of the figures in this article are available online at <http://ieeexplore.ieee.org>.

Digital Object Identifier 10.1109/TCST.2020.2981571

fundamental frequency. Moreover, Busawon and Kabore [18] proposed a proportional–integral observer in order to mitigate the effects of high-frequency measurement noises or modeling errors; however, the performance regarding FVSD is not dedicatedly discussed.

Grid-connected Converters (GcCs) have various types of industrial applications, such as grid-integrated renewable energy generation systems [19], microgrid systems [20], and uninterruptible power supplies [21]. In practice, various disturbed regimes have to be taken into account regarding the control design of GcCs. First, the transient voltage sags and long-term voltage unbalances commonly happen in power systems [22], and the unbalanced voltages then cause second-order harmonics to appear in the control systems. Besides, the power electronics devices and industrial nonlinear loads are largely penetrated the power grid, which induces large harmonics in the control system of GcCs [19], [23]. The voltage offset introduced by the offset of signal measurements or conversion circuits cannot be neglected as well [24]. Also, the power fluctuations can lead to grid frequency deviations from the nominal value (50 or 60 Hz) [25]. Note that the grid frequency deviations are limited by international standards [25], [26]. Key features of the disturbances present in GcCs are summarized as follows: 1) they are very FVSDs and 2) their frequencies are roughly known, being positive integer multiples of grid fundamental frequency.

Regarding the conventional ESO or the higher order GESO, neither of them can efficiently identify such FVSD. Then, the performances of resulting GcCs control systems would be seriously affected. Take a three-phase phase-locked loop (PLL) control system, for example, it is commonly employed to achieve the grid synchronization for GcCs [24], [27]. The ESO-based PLL can achieve satisfying performance if no harmonics pollute the control system [28]. In practice, grid voltages are not pure balanced sinusoids but disturbed by unbalances, harmonics, and voltage offsets [19], [22]–[24]. The harmonics components then appear in the estimated output phase angle. Finally, the control performance of GcCs is degraded due to the bad-quality output of a PLL. In addition, the SRF-PLLs are commonly equipped with additional filters under disturbed regimes [28], such as decoupled PLL (DPLL) [29] and moving average filter PLL (MAF-PLL) [30]. The DPLL can deal with the unbalanced grid perfectly, and the results for harmonics polluted grids are practically accepted but not satisfactory [29]. The MAF-PLL, however, presents a slow dynamic response [30]. More critically, neither of them can effectively deal with the voltage offset. A generalized integrator-ESO (GI-ESO) is, thus, proposed in this article, which then can be employed to address such issues for its applications into GcCs.

GI, also known as a resonant controller, has been widely used for different purposes [19], [23], [31], [32]. In this work, a GI-ESO is developed from conventional ESO. The pure integrator is maintained to track the direct current (dc)-type or very low-frequency disturbances. Besides, GIs of different resonant frequencies are inserted into the disturbance estimation loop to deal with the FVSD. Furthermore, a frequency-adaptive mechanism is introduced in order to mitigate the effects of frequency deviations. This design enables FVSD to be observed

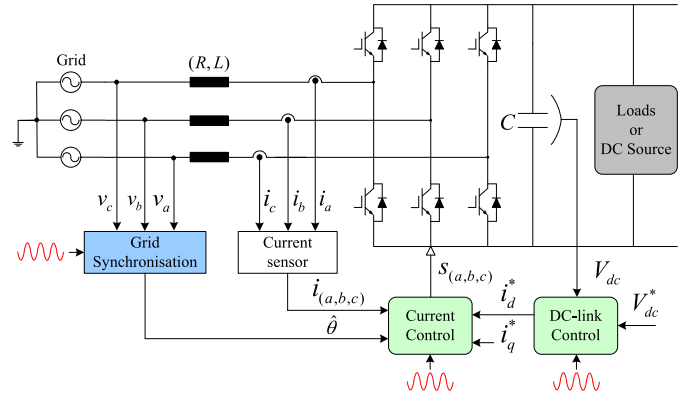


Fig. 1. Schematic of a disturbed GcC with the commonly used control structure, with $i_{(abc)}$ being the grid currents, $v_{(abc)}$ the grid voltages, i_d^* and i_q^* the d -axis and the q -axis grid current references, V_{dc} the dc-link voltage, C the dc-link capacitance, L and R the filter inductance and resistance, respectively, and $S_{(a,b,c)}$ the switching states.

with a relatively low bandwidth, which resolves the tradeoff between the bandwidth of ESO and the high-frequency noises filtering. A three-phase PLL control system under disturbed regimes is chosen as an example to assess the effectiveness of the proposed GI-ESO and the stability of the resulting control system.

This article is organized as follows. The problem formulation is described in Section II, and a case of three-phase PLL system is, in particular, chosen as an example to formulate the control issues. The proposed GI-ESO is designed and then applied to the three-phase PLL system in Section III; meanwhile, the control stabilities and the tuning guidelines are discussed in detail. Then, experimental results under various disturbed regimes are provided to assess its effectiveness in Section IV. Concluding remarks are provided in Section V.

II. PROBLEM FORMULATION

A disturbed GcC with its commonly used control structure is illustrated in Fig. 1. The control of GcCs primarily has three functions: the grid synchronization [28], the grid current control [19], and the dc-link voltage control [33]. As aforementioned in Section I, large sinusoidal disturbances could be present in the control system of GcCs under disturbed regimes. These disturbances show the following common features.

- 1) They are very FVSDs.
- 2) Their frequencies are roughly known, being positive integer multiples of the grid fundamental frequency.

The proper synchronization with grid voltage is important to ensure the whole performance of resulting GcCs control systems. In this work, the case of synchronous reference frame PLL (SRF-PLL) is chosen as an illustrative example to formulate the control issues and then to assess the effectiveness of the proposed GI-ESO.

A. SRF-PLL Modeling and Error Analysis

A common design diagram of SRF-PLL is shown in Fig. 2(a), which is composed of a phase detector (PD), a loop filter (LF), and a voltage-controlled oscillator (VCO) [27]. More design details can be found in [24], [27], [28], but some key aspects are worth to be highlighted.

- 1) The magnitude V_m acts as the gain in the forward path of the linear model, as shown in Fig. 2(b). This means that

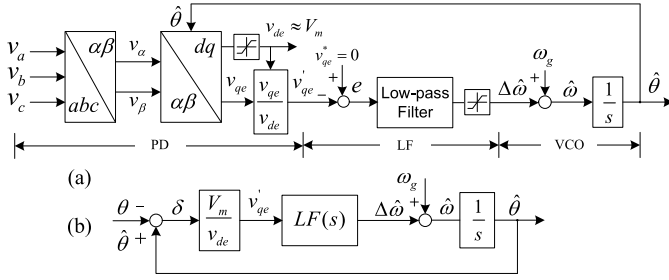


Fig. 2. (a) Schematic of conventional SRF-PLL. (b) Linear model with v_{qe} and v_{de} beign the voltages in a dq SRF, v_α and v_β the voltages in a $\alpha\beta$ rotating reference frame, V_m the grid voltage magnitude, ω_g the grid nominal angular frequency, $\hat{\omega}$ the estimated angular frequency, $\Delta\hat{\omega}$ the estimated angular frequency deviation, $\hat{\theta}$ the estimated phase angle, and $LF(s)$ the transfer function of LF.

the magnitude variations can affect the loop gain and, therefore, the stability margins and dynamic behavior of SRF-PLL, that is, the reason why a magnitude normalization scheme is usually introduced in order to decouple the effects from magnitude variations [27].

- 2) Two saturation blocks are also introduced. The saturation block of d -axis voltage is used to avoid the division by zero in the transient process. The saturation block of the controller is used to ensure that the estimated frequency meets the related international standards.

Note that ESO- or GI-ESO-based SRF-PLLs presented later also follow the abovementioned principles.

The modeling and estimation errors analysis of SRF-PLL for various disturbed regimes have been proposed in [24]. The unbalanced case is, in particular, presented in this section. The errors analysis of SRF-PLL in the presence of harmonics and voltage offsets are provided in the Appendix. The unbalanced voltages can be represented by

$$\begin{bmatrix} v_a \\ v_b \\ v_c \end{bmatrix} = V_m \begin{bmatrix} \cos\theta \\ (1+A)\cos\left(\theta - \frac{2\pi}{3}\right) \\ (1+B)\cos\left(\theta + \frac{2\pi}{3}\right) \end{bmatrix} \quad (1)$$

where A and B represent the unbalanced levels. With the Park transform [24], the q -axis voltage is given by

$$v_{qe} = V_m \sin\delta - V_m \left[\frac{A-B}{2\sqrt{3}} (\cos\theta \cos\hat{\theta} - \sin\theta \sin\hat{\theta}) + \frac{A+B}{6} (\sin\theta \cos\hat{\theta} + \cos\theta \sin\hat{\theta}) \right]. \quad (2)$$

The phase error $\delta = \hat{\theta} - \theta$ is very small ($\theta \approx \hat{\theta}$) and $\theta + \hat{\theta} \approx 2\theta$; the expression can be rewritten by

$$v_{qe} \approx V_m [\delta - E_{2\omega} \cos(2\theta + \phi_{ub})] \quad (3)$$

where

$$E_{2\omega} = \sqrt{\left(\frac{A-B}{2\sqrt{3}}\right)^2 + \left(\frac{A+B}{6}\right)^2}$$

$$\phi_{ub} = -\tan^{-1}\left(\frac{1}{\sqrt{3}} \frac{A+B}{A-B}\right).$$

Under an unbalanced grid condition, the sinusoidal disturbances would be transmitted to the output phase angle [24].

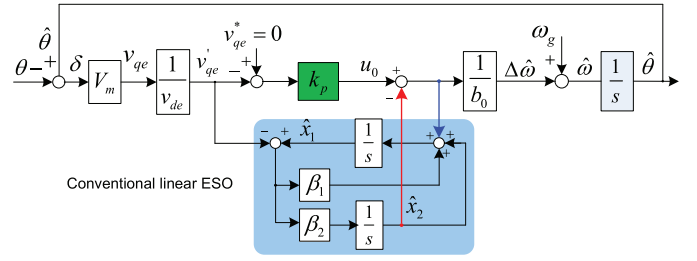


Fig. 3. Conventional ESO-based SRF-PLL control diagram. \hat{x}_1 is the estimation of v'_{qe} , \hat{x}_2 is the estimation of total unknown disturbances, β_1 and β_2 are the tuned positive gains of ESO, and b_0 is the estimation of control gain.

The phase error caused by the voltage unbalances can be expressed as follows:

$$0 < |\delta| \leq E_{2\omega} |\cos(2\theta + \phi_{ub})|. \quad (4)$$

B. ESO-Based SRF-PLL Design Principles and Its Limitations

An ESO-based controller is used in order to enhance the control dynamics of SRF-PLLs in [28]. First, the design principles are briefly reviewed. Then, the ESO's limitations when used in disturbed grids are analyzed and experimentally revealed.

The control diagram of the ESO-based SRF-PLL is shown in Fig. 3, where an ESO-based corrector is used as the LF. ESO is used to track the unknown disturbances in the PLL system. The estimated disturbances \hat{x}_2 are actively compensated into the signal u_0 in real time.

The first step before using an ESO-based controller is to reformulate a practical control issue in the canonical form of cascaded integrators with generalized disturbances [8]. By differentiating and simply manipulating the expression (3), the canonical form becomes

$$\frac{1}{V_{de}} \frac{dv_{qe}}{dt} = \frac{V_m}{V_{de}} \frac{d(\hat{\theta} - \theta)}{dt} = b_0 \Delta\hat{\omega} + f. \quad (5)$$

An appropriate disturbance definition is critical to achieve a high-efficiency ESO [8]. In the PLL, v_{de} stands for the real-time estimation of V_m ; therefore, the control gain $b = V_m/v_{de}$ approximates 1. It is reasonable to set the estimation of control gain with $b_0 = 1$. Moreover, the nominal grid frequency ω_g is feedforwarded in the control input. Such compensation improves ESO estimation's precision and response dynamics. Finally, the total disturbances f is formulated by

$$f = [(b - b_0)\Delta\hat{\omega} + (\omega_g - \omega) + d_x] + 2\omega E_{2\omega} \sin(2\theta + \phi_{ub}) = d_{(0)} + d_{(2\omega)} \quad (6)$$

where $d_{(0)} = (b - b_0)\Delta\hat{\omega} + (\omega_g - \omega) + d_x$, $(b - b_0)\Delta\hat{\omega}$ is due to the small mismatch between b and b_0 , $\omega_g - \omega$ is the grid frequency variations, and d_x represents extra disturbances, such as low-frequency disturbances induced by phase jumps, time-varying parameters, and nonlinear dynamics; $d_{(2\omega)} = 2\omega E_{2\omega} \sin(2\theta + \phi_{ub})$ represents the harmonics disturbances.

To highlight, the frequency deviations, the voltage magnitude variations, and phase jumps have a physically limited changing rate in the power system, such as the majority of related signals. For instance, the frequency jump is related to

the speed variations of the synchronous generators that have their inertia. For the inrush currents and voltages, the phase jump can be considered as ramps even for a phenomenon with a very short interval time. In conclusion, the signals that we are referring to are differentiable with bounded derivatives.

In the sequel, the following definitions are used: $\Delta\hat{\omega}$ is the control input u , v_{qe}^* is the reference r , v_{qe}' is the output y , which is defined as a state variable by $x_1 = v_{qe}'$, f is treated as an extended state variable and expressed by $x_2 = f$, and its time derivative is given by $\dot{x}_2 = h$ [28]. Now, the state-space model can be constructed as follows:

$$\begin{bmatrix} \dot{x}_1 \\ \dot{x}_2 \end{bmatrix} = \begin{bmatrix} 0 & 1 \\ 0 & 0 \end{bmatrix} \begin{bmatrix} x_1 \\ x_2 \end{bmatrix} + \begin{bmatrix} b_0 \\ 0 \end{bmatrix} u + \begin{bmatrix} 0 \\ 1 \end{bmatrix} h. \quad (7)$$

Based on (7), the ESO can be formulated as follows:

$$\begin{bmatrix} \dot{\hat{x}}_1 \\ \dot{\hat{x}}_2 \end{bmatrix} = \begin{bmatrix} 0 & 1 \\ 0 & 0 \end{bmatrix} \begin{bmatrix} \hat{x}_1 \\ \hat{x}_2 \end{bmatrix} + \begin{bmatrix} b_0 \\ 0 \end{bmatrix} u + \begin{bmatrix} \beta_1 \\ \beta_2 \end{bmatrix} [x_1 - \hat{x}_1] \quad (8)$$

where \hat{x}_1 is the estimation of v_{qe}' , \hat{x}_2 is the estimation of total disturbances, and β_1 and β_2 are the positive gains of ESO.

By subtracting (8) from (7), the error dynamics are defined by

$$\begin{bmatrix} \dot{e}_1 \\ \dot{e}_2 \end{bmatrix} = \underbrace{\begin{bmatrix} -\beta_1 & 1 \\ -\beta_2 & 0 \end{bmatrix}}_{A_e} \begin{bmatrix} e_1 \\ e_2 \end{bmatrix} + \begin{bmatrix} 0 \\ 1 \end{bmatrix} h \quad (9)$$

where $e_1 = x_1 - \hat{x}_1$ is the state estimation error, and $e_2 = x_2 - \hat{x}_2$ is the disturbances estimation error. The positive gains $\beta_1 = 2\omega_o$ and $\beta_2 = \omega_o^2$ are chosen such that the characteristic polynomial (10) is the Hurwitz stable [4]

$$\lambda(s) = (sI - A_e)^{-1} = s^2 + \beta_1 s + \beta_2 = (s + \omega_o)^2 \quad (10)$$

where ω_o is referred to as the bandwidth of ESO [4].

Based on Fig. 3, the control law is formulated by

$$\Delta\hat{\omega} = \frac{k_p(v_{qe}^* - v_{qe}') - \hat{x}_2}{b_0}. \quad (11)$$

If the total disturbances were correctly estimated and compensated, the original plant model would be reduced to be a pure integrator [34]. Then, the closed-loop transfer function can be approximated by

$$H_c(s) \approx \frac{k_p \frac{1}{s}}{1 + k_p \frac{1}{s}} = \frac{1}{1 + \frac{s}{k_p}} \quad (12)$$

where $\omega_c \approx k_p$ is referred to as the closed-loop bandwidth.

More details on convergence analysis, stability analysis, and tuning methods can be found in [4], [7], [34], and [35].

C. ESO's Limitations in Tracking the FVSD

Based on (9), the transfer function of disturbances estimation error becomes

$$f_{e_2}(s) = \frac{e_2(s)}{f(s)} = \frac{s(s + 2\omega_o)}{(s + \omega_o)^2}. \quad (13)$$

The Bode plots of $f_{e_2}(s)$ are shown in Fig. 4, with $\omega_o \in \{300, 400, 500\}$ (rad/s). It can be observed that ESO behaves like a low-pass filter with respect to the input disturbances [34]. The conventional ESO can estimate the unknown disturbance very well only when the disturbances are composed of low-frequency components. The estimation errors of disturbances can be reduced by increasing the bandwidth ω_o ;

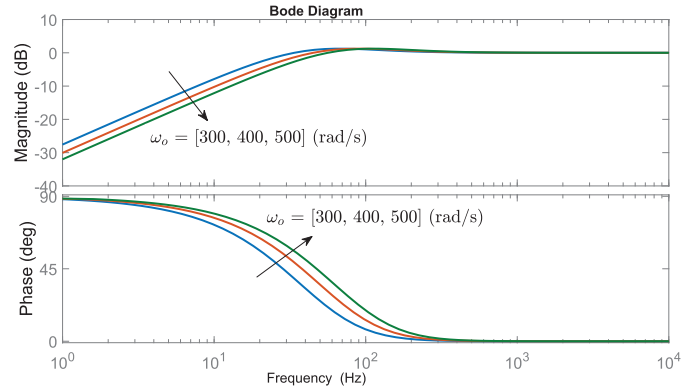


Fig. 4. Bode diagram of the transfer function $f_{e_2}(s)$.

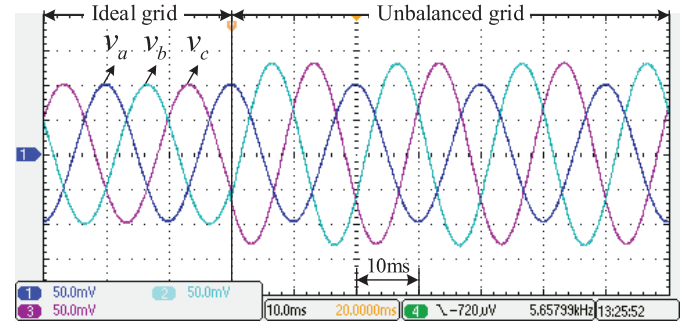


Fig. 5. Three phase voltages: v_a , v_b , and v_c (50 V/div).

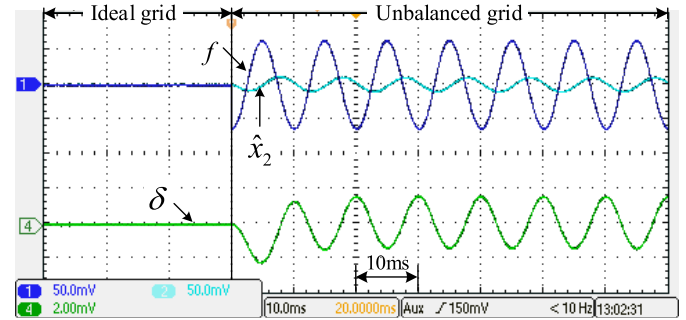


Fig. 6. Performance of conventional ESO-based SRF-PLL. f is the total disturbances (50/div), \hat{x}_2 is the estimated disturbances by ESO (50/div), and δ is the estimated phase error (2° /div).

however, the bandwidth would be limited by the practical noises.

Experimental results are obtained by using the dSPACE controller (DS2005). Three-phase voltages are configured, as shown in Fig. 5: at the beginning, three-phase voltages are considered to be balanced with $V_m = 100$ V, and $A = B = C = 0\%$; then, the unbalanced regime is set to $V_m = 100$ V, $A = 0\%$, $B = 30\%$, and $C = 30\%$.

Following the tuning rules as [28], the control parameters are configured with $\omega_c = 100$ rad/s and $\omega_o = 400$ rad/s. The results of ESO-based SRF-PLL are shown in Fig. 6. The grid phase angle is correctly estimated for the ideal grid, while the phase estimation errors are not negligible in the presence of grid unbalances. The reason is that the total disturbances defined by (6) are partially filtered by ESO, and the second-order harmonics are then introduced into the estimated phase angle.

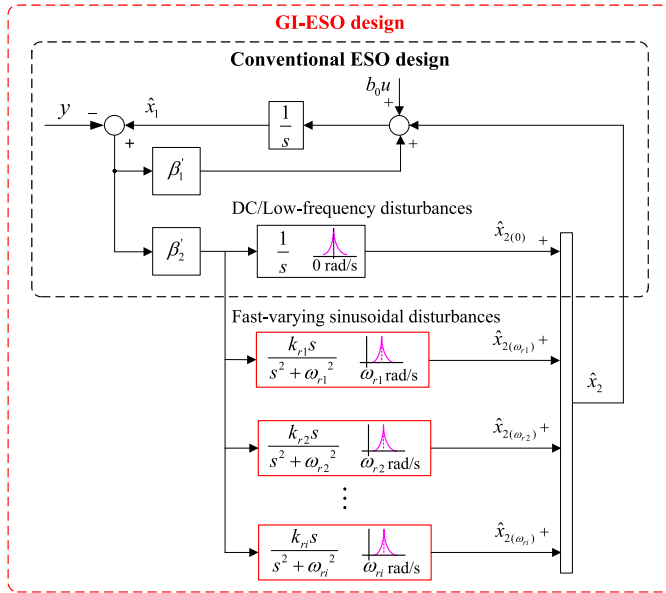


Fig. 7. Proposed GI-ESO design diagram.

The ESO-based PLL can also be equipped with additional filters under disturbed regimes, such as DPLL and MAF-PLL, but neither of them can efficiently deal with the voltage offsets. A GI-ESO is, therefore, proposed to address such issues for its applications into GcCs.

III. GI-ESO DESIGN AND ITS APPLICATION TO SRF-PLL

In this section, the main properties of GI-ESO are first highlighted. Then, a GI-ESO-based SRF-PLL is designed in order to assess the performance of the proposed GI-ESO and the stability of its resulting control system.

A. GI-ESO Design

The GI-ESO is developed from the previous linear ESO. It inherits the ESO's original advantages: high robustness, good disturbance rejection abilities within the bandwidth of ESO, and simple tuning methods [4]. More critically, the capability in dealing with FVSD is enhanced for the proposed GI-ESO.

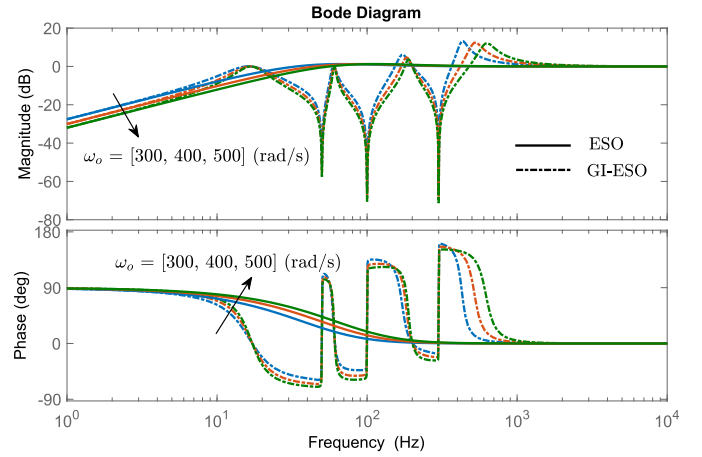
B. Extended Structure and Mathematical Model

The proposed GI-ESO and the conventional ESO are comparatively presented in Fig. 7. The pure integrator in the disturbance loop is kept to track dc-type or very low-frequency disturbances due to the infinite gain of the pure integrator at zero frequency [31]. Moreover, the GIs of selective resonant frequencies are inserted in parallel in order to observe the FVSD of different frequencies.

The inserted GI can be generally expressed by (14), wherein the infinite gain of the integrator is shifted to ω_{r_i} [31]

$$R_i(s) = \frac{k_{r_i} s}{s^2 + \omega_{r_i}^2}, \quad i = 1, 2, \dots \quad (14)$$

where k_{r_i} is the proportional gain and ω_{r_i} is the selective resonant frequency of each GI.


 Fig. 8. Bode diagram of the transfer function $F_{e_2}(s)$.

A GI-ESO is extended from a conventional ESO (8) by

$$\begin{bmatrix} \dot{\hat{x}}_1 \\ \dot{\hat{x}}_2 \end{bmatrix} = \begin{bmatrix} 0 & 1 \\ 0 & 0 \end{bmatrix} \begin{bmatrix} \hat{x}_1 \\ \hat{x}_2 \end{bmatrix} + \begin{bmatrix} b_0 \\ 0 \end{bmatrix} u + \begin{bmatrix} \beta'_1 \\ \beta'_2(1 + R(s)) \end{bmatrix} [x_1 - \hat{x}_1] \quad (15)$$

where $\hat{x}_2 = \hat{x}_{2(0)} + \hat{x}_{2(\omega_{r_1})} + \hat{x}_{2(\omega_{r_2})} + \dots + \hat{x}_{2(\omega_{r_i})}$ is the total estimated disturbances, and $R(s)$ is a general expression that is $R(s) = 0$ for ESO; $R(s) = R_1(s) + R_2(s) + \dots + R_i(s)$ for GI-ESO. The observer gains are expressed by $\beta'_1 = \zeta\omega_0$, $\beta'_2 = \omega_0^2$, and ζ is the tuning coefficient. Detailed theoretical analysis and selection guidelines are provided later in the sequel.

C. Estimation Error Assessment

Similarly, by subtracting (15) from (7), the estimation errors can be expressed by

$$\begin{bmatrix} \dot{e}_1 \\ \dot{e}_2 \end{bmatrix} = \begin{bmatrix} -\beta'_1 & 1 \\ -\beta'_2(1 + R(s)) & 0 \end{bmatrix} \begin{bmatrix} e_1 \\ e_2 \end{bmatrix} + \begin{bmatrix} 0 \\ 1 \end{bmatrix} h. \quad (16)$$

By replacing h with $\dot{f}(s)$, the transfer function between $e_2(s)$ and $f(s)$ becomes

$$F_{e_2}(s) = \frac{s(s + \zeta\omega_0)}{s^2 + \zeta\omega_0 s + \omega_0^2(1 + R(s))}. \quad (17)$$

The Bode plots of $F_{e_2}(s)$ are shown in Fig. 8, in which the disturbance estimation errors of ESO and GI-ESO are comparatively presented. For these two observers, the bandwidth is set to $\omega_o \in \{300, 400, 500\}$ (rad/s), and $\zeta = 5$. The inserted GIs are, respectively, set to $k_{r_1} = \pi$, $\omega_{r_1} = \omega_g$ for voltage offset, $k_{r_2} = 5\pi$, $\omega_{r_2} = 2\omega_g$ for unbalanced grids, $k_{r_3} = 10\pi$, $\omega_{r_3} = 6\omega_g$ for the fifth- and seventh-order harmonics (proven in the Appendix), and $\omega_g = 100\pi$ rad/s. The Bode plots indicate that GI-ESO and ESO performs closely at either the very low- or high-frequency range. Moreover, being different from ESO, the proposed GI-ESO can also correctly track very FVSD. The reason is that the inserted GIs enable rather high gains at specific resonant frequencies.

D. GI-ESO-Based SRF-PLL Design

The primary principles described in Section II-B are followed here; moreover, several particular points are highlighted.

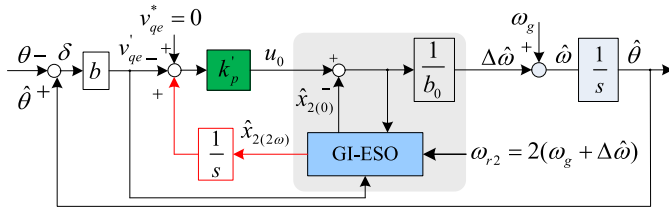


Fig. 9. GI-ESO-based SRF-PLL under voltage unbalances.

E. Disturbances Compensation

It has been proven in Section III-A that the proposed GI-ESO is capable of estimating very FVSDs. However, another key question is how to correctly compensate for the estimated disturbances. The GI-ESO-based SRF-PLL control diagram is shown in Fig. 9. The phase angle is indirectly estimated by controlling the q -axis voltage. If the total disturbances were compensated by the control signal $\Delta\omega$, the second-order frequency components would remain in the estimated frequency $\hat{\omega}$ and the output phase $\hat{\theta}$. Since the information of phase and frequency is more important in a PLL system, we can force the harmonics components to stay in the q -axis voltage (see Fig. 9). It comes from (3) that the integration of $\hat{x}_{2(2\omega)}$ actually represents the v_{qe} fluctuations caused by unbalanced voltages. Finally, the sinusoidal errors can be actively removed from the output estimated phase.

F. Frequency-Adaptive Mechanism

Note that the actual grid frequency possibly derives from its nominal value ω_g [25]. If the resonant frequency of GI is set to be constant, then the performances of GI-ESO when used in GcCs can be deteriorated. A frequency-adaptive mechanism is, hence, considered in this design (see Fig. 9). For example, under voltage unbalances, the value of the resonant frequency of GI is adaptively adjusted by considering the estimated frequency deviation with $\omega_{r2} = 2(\omega_g + \Delta\hat{\omega})$. As the applied resonant frequencies of GIs are corrected in real time, the negative effects induced by frequency deviations can be significantly mitigated.

G. Control Law Formulation

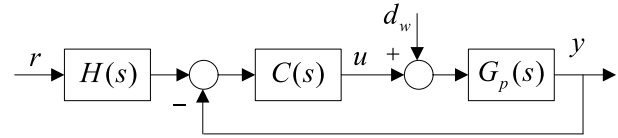
The dc-type or low-frequency disturbances $\hat{x}_{2(0)}$ are directly compensated in the signal u_0 . The integration of $\hat{x}_{2(2\omega)}$ is added to the q -axis voltage reference. Finally, the modified control law is expressed by

$$\Delta\hat{\omega} = \frac{k'_p(v_{qe}^* + \int \hat{x}_{2(2\omega)} dt - v_{qe}') - \hat{x}_{2(0)}}{b_0}. \quad (18)$$

The GI-ESO handles all sinusoidal components that are present in the SRF-PLL as generalized disturbances. The structure of GI-ESO can be flexibly adapted to different disturbed regimes by adjusting the selective frequencies.

H. Stability Analysis

The stability index is a crucial factor in evaluating the quality of a controller. Stabilities analysis methods of ESO can be referred for that of GI-ESO [35]–[37]. The frequency-domain properties are, therefore, quantitatively analyzed in this section. This is done under the following assumptions.

Fig. 10. 2dof closed-loop diagram of GI-ESO-based SRF-PLL control system. d_w represents the external disturbances.

- 1) A mismatch between b and b_0 is assumed, and the control gain is set to be $b = 1.2$ and $b_0 = 1$.
- 2) The parameters k_{r1} and ω_{r1} are defined as the proportional gain and the resonant frequency for the GI dealing with voltage offsets, similarly ω_{r2} and k_{r2} for voltage unbalances, and ω_{r3} and k_{r3} for harmonics.
- 3) Phase margins around 45° are supposed to be acceptable.

From expressions (15) and (18), the transfer function can be obtained

$$\frac{u(s)}{y(s)} = -\frac{1}{b_0} \frac{\omega_c s^2 + \omega_o^2 s + \zeta \omega_o \omega_c s + \omega_o^2 \omega_c}{s(s + \zeta \omega_o) + \omega_o^2(s + \omega_c)R(s)} \quad (19)$$

$$\frac{u(s)}{r(s)} = \frac{1}{b_0} \frac{\omega_c s^2 + \omega_o^2 \omega_c R(s)s + \zeta \omega_o \omega_c s + \omega_o^2 \omega_c}{s(s + \zeta \omega_o) + \omega_o^2(s + \omega_c)R(s)} \quad (20)$$

where $r(s)$, $u(s)$, and $y(s)$ are the Laplace transforms of $r = v_{qe}^*$, $u = \Delta\hat{\omega}$, and $y = v_{qe}'$, respectively.

By introducing the following notations:

$$C(s) = \frac{1}{b_0} \frac{\omega_c s^2 + \omega_o^2 s + \zeta \omega_o \omega_c s + \omega_o^2 \omega_c}{s(s + \zeta \omega_o) + \omega_o^2(s + \omega_c)R(s)} \quad (21)$$

$$H(s) = \frac{\omega_c s^2 + \omega_o^2 \omega_c R(s)s + \zeta \omega_o \omega_c s + \omega_o^2 \omega_c}{\omega_c s^2 + \omega_o^2 s + \zeta \omega_o \omega_c s + \omega_o^2 \omega_c} \quad (22)$$

the ESO-based controller can be formulated to a two-degree-of-freedom (2dof) closed-loop system, as shown in Fig. 10. Now, the feedback control loop has a standard structure of the feedback and the controlled plant [37].

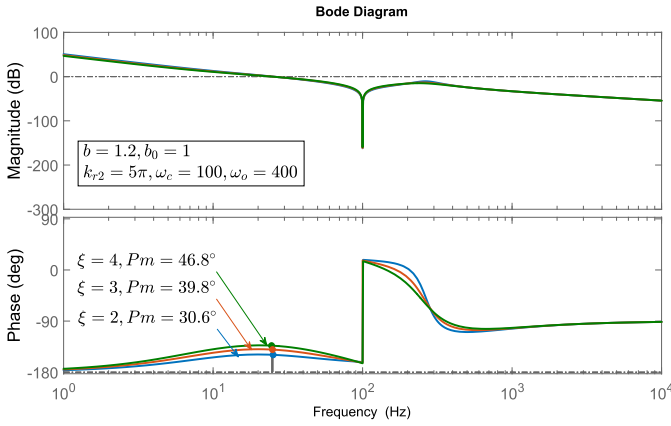
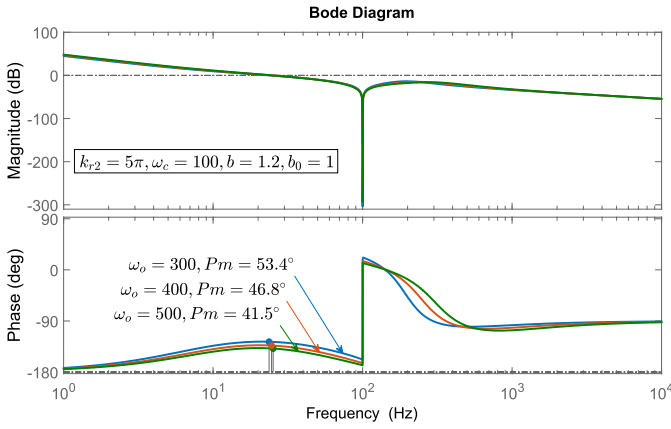
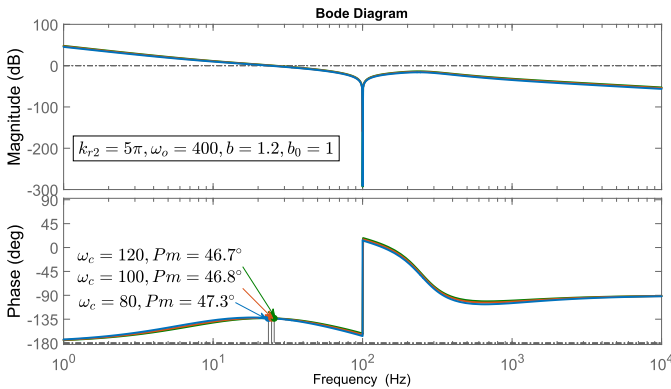
First, the phase margins of the loop transfer function of the controlled system are discussed. The loop transfer function is given by

$$\begin{aligned} L(s) &= C(s)G_p(s) \\ &= \frac{1}{b_0} \frac{\omega_c s^2 + \omega_o^2 s + \zeta \omega_o \omega_c s + \omega_o^2 \omega_c}{s(s + \zeta \omega_o) + \omega_o^2(s + \omega_c)R(s)} \frac{b}{s} \end{aligned} \quad (23)$$

where the plant model is $G_p(s) = b/s$, and $b = V_m/v_{de}$.

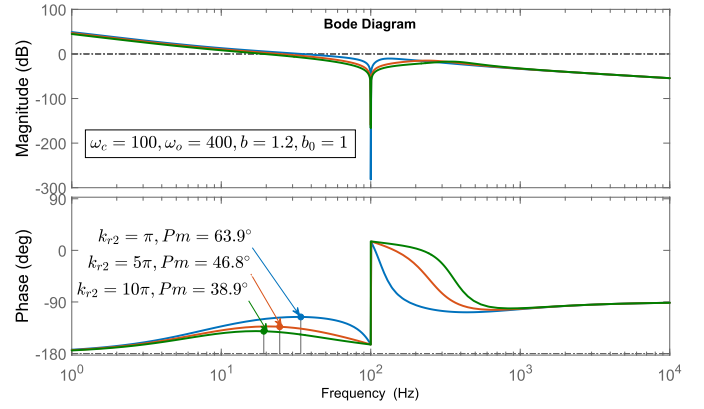
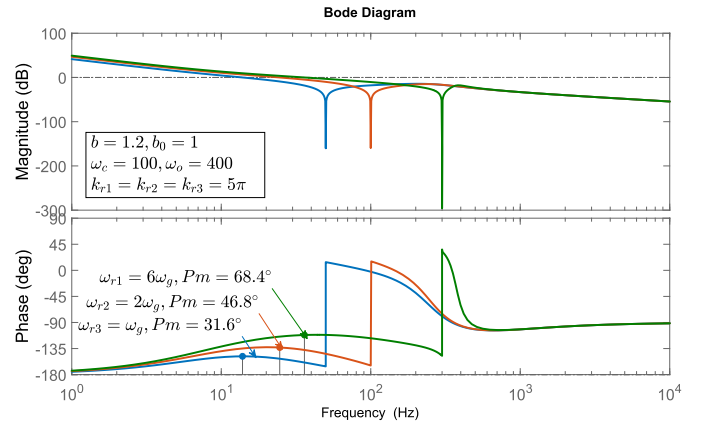
The unbalanced voltage case is exclusively studied in order to analyze the effects on stability with respect to each parameter (ζ , ω_o , ω_c , and k_r). The Bode plots of $L(s)$ for different coefficients $\zeta \in \{2, 3, 4\}$ are shown in Fig. 11. The remaining parameters are set to $\omega_o = 400$ rad/s, $\omega_c = 100$ rad/s, $k_{r2} = 5\pi$, and $\omega_{r2} = 2\omega_g$. It can be observed that the gain margin is negative infinite; however, the phase margin cannot sufficiently meet stabilities requirements for $\zeta = 2$ or $\zeta = 3$, while too large ζ enables slow dynamics response [4]. Therefore, $\beta'_1 = 4\omega_0$ and $\beta'_2 = \omega_0^2$ are chosen in this work as well as in the forthcoming analysis.

The Bode plots of $L(s)$ for different ω_o and ω_c are shown in Figs. 12 and 13, respectively. The GI is applied with $k_{r2} = 5\pi$ and $\omega_{r2} = 2\omega_g$. The ESO's tuning rule can be referred, which is commonly configured by $\omega_o = 3 \sim 5\omega_c$ [4]. Then, we make the following settings: $\omega_o \in \{300, 400, 500\}$

Fig. 11. Bode plots of $L(s)$ for coefficient $\zeta \in \{2, 3, 4\}$.Fig. 12. Bode plots of $L(s)$ for $\omega_o \in \{300, 400, 500\}$ (rad/s).Fig. 13. Bode plots of $L(s)$ for $\omega_c \in \{80, 100, 120\}$ (rad/s).

(rad/s) and $\omega_c = 100$ rad/s for Fig. 12, and $\omega_o = 400$ (rad/s) and $\omega_c \in \{80, 100, 120\}$ (rad/s) for Fig. 13. It can be seen that the phase margin will decrease with larger observer bandwidth ω_o , which can deteriorate stabilities of the closed-loop control system. However, the phase margins are insensitive to the changes of ω_c .

The Bode plots of $L(s)$ of different k_{r2} are shown in Fig. 14. The GIs are set to $k_{r2} \in \{\pi, 5\pi, 10\pi\}$, and $\omega_{r2} = 2\omega_g$. Larger k_{r2} enables higher gains of GI at the selective frequencies, which helps improving the estimation accuracy of GI-ESO. However, the phase margins are sensitive to the changes of k_{r2} , as shown in Fig. 14. The high gains tend to bring destabilizing

Fig. 14. Bode plots of $L(s)$ for $k_{r2} \in \{\pi, 5\pi, 10\pi\}$.Fig. 15. Bode plots of $L(s)$ for various selective frequencies.

effects on the resulting closed-loop system. Too large gains would be risky with respect to stability issues. Consequently, the gains of inserted GI are limited accordingly.

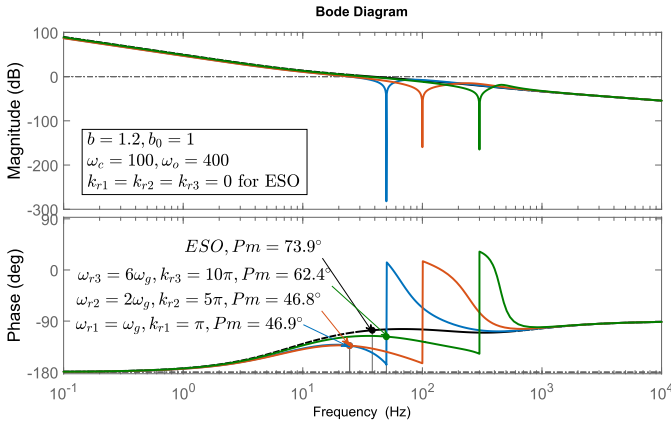
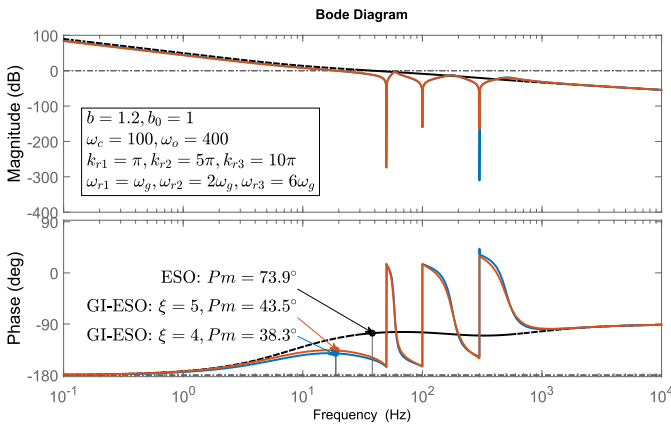
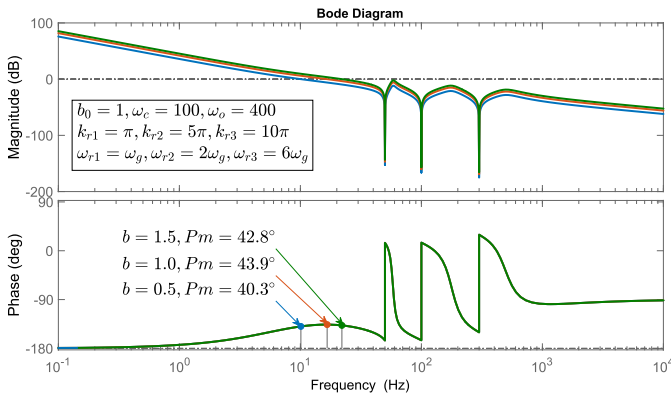
Now, the stabilities of GI-ESOs with different selective frequencies are analyzed. The resonant frequencies of applied GIs are, respectively, configured with $\omega_{r1} = \omega_g$ for voltage offset, $\omega_{r2} = 2\omega_g$ for grid unbalance, and $\omega_{r3} = 6\omega_g$ for fifth- and seventh-order harmonics (see the Appendix).

The Bode plots of $L(s)$ for different selective frequencies are provided in Fig. 15. The same gains of GIs with $k_{r1} = k_{r2} = k_{r3} = 5\pi$ are used. It can be seen that the phase margin decreases critically for a system that applies a GI with a lower resonant frequency. Therefore, the gains of GIs must be selected by taking into account its applied resonant frequency.

Fig. 16 shows the Bode plots of $L(s)$ that apply different gains k_{ri} , and the remaining parameters keep the same configurations. Compared with the ESO, although the stability margins decrease due to the high gains of GIs, the stability condition can be ensured by properly adjusting k_{ri} .

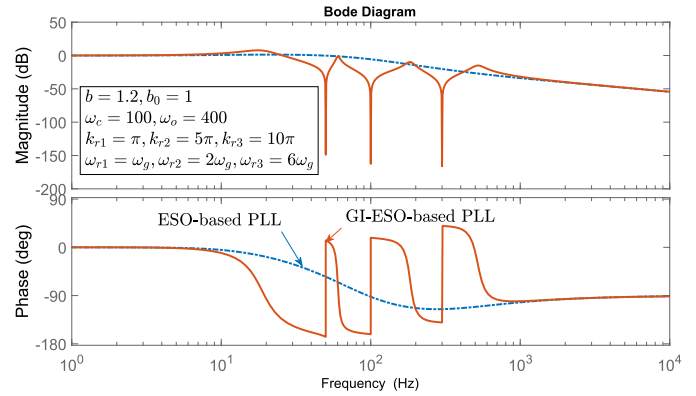
The Bode plots of $L(s)$ for multi-GIs in parallel are provided in Fig. 17, with the same parameters settings as that applied in Fig. 16. It can be observed that multi-GIs cause a further decrease in the phase margin ($\zeta = 4$, $P_m = 38.3^\circ$). The coefficient ζ is, thus, adjusted by using $\zeta = 5$ for multi-GIs to ensure that the stability margin is sufficient.

The control system performances and stability can be affected by model uncertainties. The main uncertain parameter

Fig. 16. Bode plots of $L(s)$ for a different value of k_{r_i} .Fig. 17. Bode plots of $L(s)$ for multiple selective frequencies.Fig. 18. Bode plots of $L(s)$ for $b \in \{0.5, 1, 1.5\}$.

is the control gain b . The estimation of b is set to $b_0 = 1$, and the control robustness with a group of values $b \in \{0.5, 1, 1.5\}$ are successively tested. The Bode plots of the loop transfer function $L(s)$ for different b are provided in Fig. 18. The phase margin decreases when b_0 is far from the real value of b . However, the phase margin are insensitive to variations of b and remain always practically accepted ($P_m > 40^\circ$).

The stability of the prefilter $H(s)$ (22) is guaranteed, as all coefficients in its denominator are positive [35]. Therefore, the closed-loop stability of the loop that linked the synthesized reference signal $r^* = \int \hat{x}_{2(2\omega)} dt + v_{qe}^*$ to the output can be

Fig. 19. Bode bolts of closed-loop transfer function $G_{cl}(s)$.TABLE I
CONFIGURATIONS OF CONTROL PARAMETERS

Common parameters	$\omega_c = 100$ rad/s, $\omega_o = 400$ rad/s, $b_0 = 1$
Coefficient ξ	$\xi = 4$ for single GI, $\xi = 5$ for multi-GIs
Offsets	$k_{r1} = \pi$, $\omega_{r1} = (\omega_g + \Delta\hat{\omega})$
Unbalances	$k_{r2} = 5\pi$, $\omega_{r2} = 2(\omega_g + \Delta\hat{\omega})$
Harmonics	$k_{r3} = 10\pi$, $\omega_{r3} = 6(\omega_g + \Delta\hat{\omega})$

determined by

$$G_{cl}(s) = \frac{C(s)G_p(s)}{1 + C(s)G_p(s)}. \quad (24)$$

The Bode plots of $G_{cl}(s)$ are shown in Fig. 19; the same parameters are configured as that of Fig. 17. The Bode plots show that GI-ESO inherits the ESO's original properties. The closed-loop performances of ESO- and GI-ESO-based control systems behave closely at either very low- or high-frequency range. Moreover, by using a GI-ESO, the selective sinusoidal disturbances are effectively removed from the control signal as well as the output estimated phase.

This section provides a general stability analysis methodology, which can be adapted to future implementations of GI-ESOs.

I. Parameter Selection Guidelines

First, the structure and the selective frequencies of GI-ESOs need to be adapted to the sinusoidal disturbances present in real applications. Then, proper parameters have to be selected by taking into account several factors: system stability, estimation's precision, and response dynamics. The parameter tuning guidelines are summarized as follows.

- 1) First, regarding parameters ω_c and ω_0 , similar tuning rules discussed in [4] and [7] can be followed.
- 2) Then, ω_{r_i} is chosen by adapting to frequencies of the present sinusoidal disturbances, and k_{r_i} is tuned to ensure both the estimation precision and the stability.
- 3) Moreover, the coefficient ξ has to be corrected for GI-ESO to ensure the stability condition.
- 4) Finally, the applied control parameters must be retuned and validated in the experimental tests.

Finally, the control parameters are configured as given in Table I, which will be validated in the forthcoming tests.

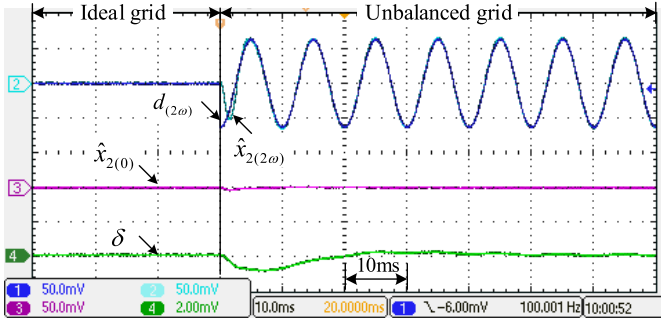


Fig. 20. Performance of GI-ESO-based PLL. $d_{(2\omega)}$ is the sinusoidal disturbances (50/div), $\hat{x}_{2(2\omega)}$ is the estimated sinusoidal disturbances (50/div), $\hat{x}_{2(0)}$ is the estimated dc-type or low-frequency disturbances (50/div), and δ is the phase error (2°/div).

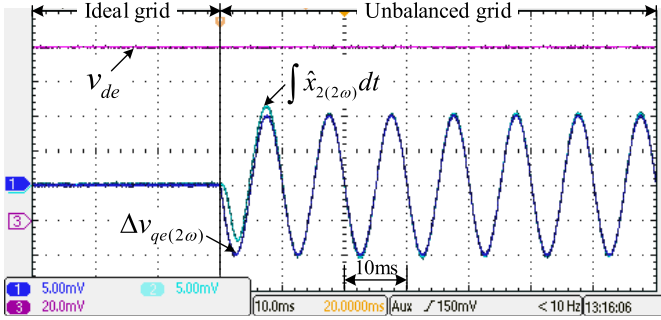


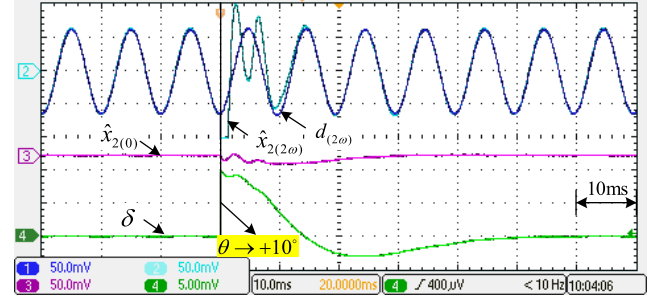
Fig. 21. Voltage components in the dq frame. $\Delta v_{qe(2\omega)}$ is the fluctuations of q -axis voltage (5 V/div), $\int \hat{x}_{2(2\omega)} dt$ is the integration of $\hat{x}_{2(2\omega)}$ (5 V/div), and v_{de} is the d -axis voltage (20 V/div).

IV. EXPERIMENTAL RESULTS AND ANALYSIS

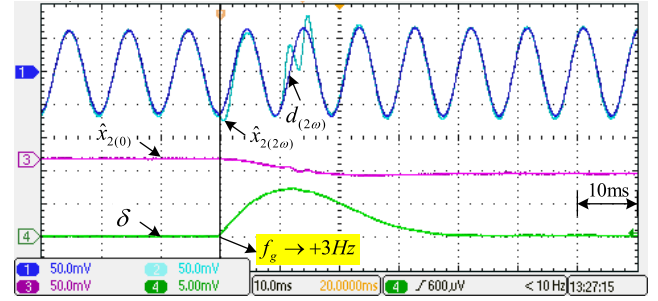
The GI-ESO-based SRF-PLL is tested in order to check the effectiveness of the proposed GI-ESO in dealing with FVSD. Various disturbed schemes (unbalances, harmonics, and voltage offset) have been considered. Experimental results are obtained by using the dSPACE controller (DS2005).

First, the grid unbalances are set to be the same as the settings in Fig. 5. The performances of GI-ESO-based PLL are shown in Fig. 20. By introducing the GI, the second-order grid frequency disturbance is approximately estimated by the GI-ESO, namely, $\hat{x}_{2(2\omega)} \approx d_{(2\omega)}$. Then, the fluctuations are actively transmitted to the q -axis voltage. Fig. 21 shows that the integration of $\hat{x}_{2(2\omega)}$ enables a tight tracking of the desired theoretical value $\Delta v_{qe(2\omega)}$. The sinusoidal components are forced to remain in the q -axis voltage. Finally, the errors are removed from the estimating phase angle. The performances are significantly improved compared with the ESO-based PLL (see Fig. 6 for comparison).

Fig. 22 provides the robustness test results of GI-ESO-based PLL for two cases: the three-phase voltages undergo a phase jump (+10°), as shown in Fig. 22(a), and a grid frequency step (+3 Hz) occurs to the grid voltages, as shown in Fig. 22(b). The GI-ESO can quickly track the sinusoidal disturbances when the external disturbances present to the grid voltage for both occasions. Moreover, the GI-ESO has a fast enough tracking performance to ensure that the control of GI-ESO-based PLL can achieve a rapid dynamic response.



(a) Phase jump +10°



(b) Frequency step +3Hz

Fig. 22. Robustness test of a GI-ESO-based PLL. $d_{(2\omega)}$ is the sinusoidal disturbances (50/div), $\hat{x}_{2(2\omega)}$ is the estimated sinusoidal disturbance (50/div), $\hat{x}_{2(0)}$ is the estimated low-frequency disturbance (50/div), and δ is the phase error (5°/div). (a) Phase jump +10°. (b) Frequency step +3 Hz.

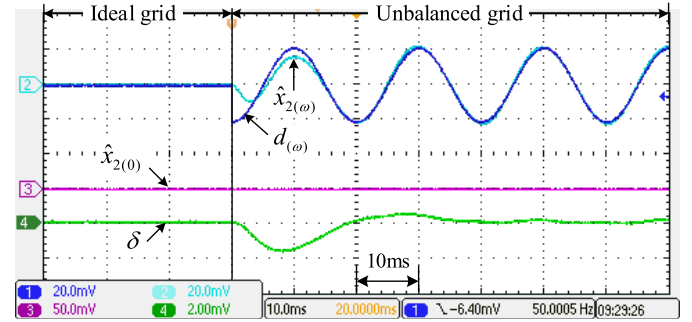


Fig. 23. Performance of GI-ESO-based PLL in the presence of voltage offset. $d_{(\omega)}$ is the sinusoidal disturbances (50/div), $\hat{x}_{2(\omega)}$ is the estimated sinusoidal disturbances (50/div), $\hat{x}_{2(0)}$ is the estimated dc or low-frequency disturbances (50/div), and δ is the phase error (2°/div).

The voltage offset is set to $V_{a0} = 0$ V and $V_{b0} = V_{b0} = 10$ V (the parameters are defined in the Appendix), and the control parameters are given in Table I. The performance of GI-ESO and the resulting PLL under voltage offset are shown in Fig. 23.

The sinusoidal disturbances induced by voltage offset have the same frequency component as that of grid voltage [24]. As shown in Fig. 23, the results indicate that the sinusoidal disturbances are tightly tracked by GI-ESO. The PLL enables performance precision regarding voltage offsets.

Regarding harmonics regime, the fifth-order harmonic of magnitude 10 V and the seventh-order harmonic of magnitude 5 V are injected simultaneously into three-phase voltages. The sixth-order harmonic disturbances appear in the SRF-PLL control system (proven in the Appendix). The control parameters are given in Table I. Fig. 24 shows that the harmonic disturbances are approximately estimated by GI-ESO.

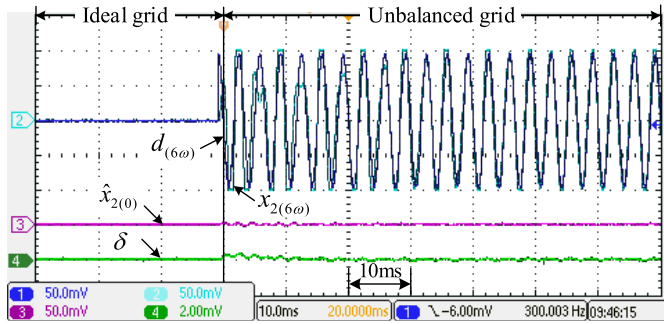


Fig. 24. Performance of GI-ESO-based PLL in the presence of harmonic disturbances. $d_{(6\omega)}$ is the sixth-order harmonic disturbances (50/div), $\hat{x}_{2(6\omega)}$ is the estimated sixth-order harmonic disturbances (50/div), $\hat{x}_{2(0)}$ is the estimated dc or low-frequency disturbances (50/div), and δ is the phase error (2° /div).

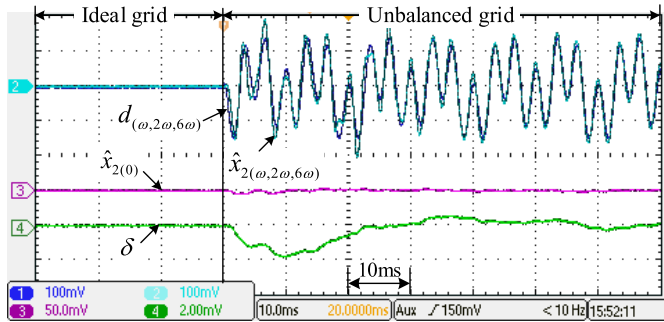


Fig. 25. Performance of GI-ESO-based PLL in the presence of multiharmonic disturbances. $d_{2(\omega,2\omega,6\omega)}$ is the multiharmonic disturbances (100/div), $\hat{x}_{2(\omega,2\omega,6\omega)}$ is the estimated disturbances (100/div), $\hat{x}_{2(0)}$ is the estimated dc or low-frequency disturbances (50/div), and δ is the phase error (2° /div).

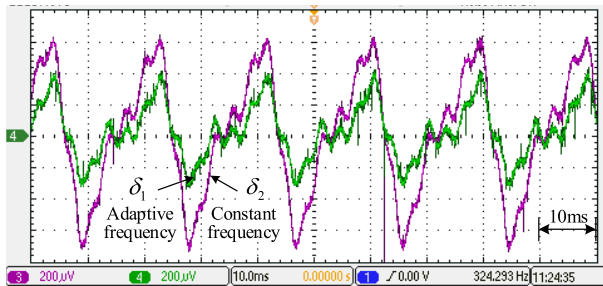


Fig. 26. Phase estimation errors in the presence of grid frequency deviation. δ_1 is the phase error with adaptive frequency (0.02° /div), and δ_2 is the phase error with fixed frequency (0.02° /div).

The high-order harmonic errors in the estimated phase become negligible.

For a real application, the PLLs are expected to be robust against unbalances, offsets, and harmonics. Fig. 25 provides the results of GI-ESO-based PLL that deals with various disturbances simultaneously. Multi-GIs of different resonant frequencies are incorporated in parallel, being configured in Table I. The total multidisturbances can be identified by the GI-ESO. The overshoot of the estimated phase angle is less than 1.1%, and the estimated phase quickly follows the phase of grid voltage. The proposed GI-ESO-based PLL achieves practically satisfying performances in the presence of various disturbances.

Fig. 26 shows the results of GI-ESO-based PLL in the presence of grid frequency deviation (+3 Hz). The comparative results indicate that the magnitude of estimated phase errors decreases by introducing the frequency-adaptive mechanism.

In this article, the presented results are focused on PLL issues. However, the proposed GI-ESO can be used in other applications that might be encountered in GcCs, such as the dc-link control or the grid current control contexts. These are topics of undergoing works.

V. CONCLUSION

This work is a development/extension of a previously proposed work on linear ESO; therefore, it inherits the ESO's original advantages. Moreover, GIs of different resonant frequencies are applied to the disturbance estimation loop, which enables FVSD to be observed with relatively low bandwidth. Besides, a frequency-adaptive mechanism is introduced in order to mitigate the effects of frequency deviations. Furthermore, the structure of GI-ESO can be flexibly adjusted regarding different disturbed regimes present on the field.

A case of the three-phase SRF-PLL control system is chosen as an example to assess GI-ESO's performance and the stability of its resulting control system. First, the frequency-domain properties, particularly the phase margins, are quantitatively analyzed with respect to different control parameters. The parameters tuning guidelines are highlighted as well. Moreover, the experimental results indicate that various FVSD can be efficiently observed by introducing GI-ESOs. The sinusoidal components are removed from the estimated phase angle by compensating correctly the estimated disturbances. Besides, in the case of frequency deviations, the frequency-adaptive mechanism mitigates the phase estimation errors. The GI-ESO also achieves high robustness under various internal or external disturbances. Both theoretical analysis and experimental results have proven the effectiveness of the proposed solution when used in GcCs in the presence of various disturbances.

The proposed GI-ESO solution breaks the limits of ESO-based controllers or ADRC for their applications in various disturbed control schemes of GcCs (grid synchronization, current control, and dc-link voltage control). Moreover, it has a wide application scope for many systems that are impacted by the presence of very FVSD. If the frequencies of sinusoidal disturbances are not known, a simple PLL can be incorporated to obtain the frequency information.

APPENDIX

ERROR ANALYSIS AND DISTURBANCES DEFINITION

The error analysis of voltage harmonics and offset is recalled in order to define the disturbances present in the control system of GI-ESO-based SRF-PLL.

A. Voltage Harmonics

The grid voltages with harmonics can be represented by

$$\begin{aligned} v_a &= V_1 \cos \theta + V_5 \cos 5\theta + V_7 \cos 7\theta + \dots \\ v_b &= V_1 \cos\left(\theta - \frac{2\pi}{3}\right) + V_5 \cos 5\left(\theta - \frac{2\pi}{3}\right) \\ &\quad + V_7 \cos 7\left(\theta - \frac{2\pi}{3}\right) + \dots \\ v_c &= V_1 \cos\left(\theta + \frac{2\pi}{3}\right) + V_5 \cos 5\left(\theta + \frac{2\pi}{3}\right) \\ &\quad + V_7 \cos 7\left(\theta + \frac{2\pi}{3}\right) + \dots \end{aligned} \quad (25)$$

where V_1, V_5, V_7, \dots represent the harmonics magnitudes.

The q -axis voltage can be derived and linearized by

$$\begin{aligned} v_{qe} &= V_1 \sin \delta + V_5 \sin(\hat{\theta} + 5\theta) + V_7 \sin 7(\hat{\theta} - 7\theta) + \dots \\ &\approx V_1 \delta + (V_5 - V_7) \sin 6\theta + (V_{11} - V_{13}) \sin 12\theta + \dots \end{aligned} \quad (26)$$

The phase error caused by voltage harmonics is given by

$$\delta = E_{6\omega} \sin 6\theta + E_{12\omega} \sin 12\theta + \dots \quad (27)$$

where

$$E_{6\omega} = \frac{V_5 - V_7}{V_1}, \quad E_{12\omega} = \frac{V_{11} - V_{13}}{V_1}, \dots$$

The voltage harmonics enables the phase errors with the frequency components of 6ω , 12ω , \dots . The total disturbance of ESO-based PLL control system can be represented by

$$\begin{aligned} f &= [(b - b_0)\Delta\hat{\omega} + (\omega_g - \omega) + d_x] \\ &\quad + 6\omega E_{6\omega} \cos 6\theta + 12\omega E_{12\omega} \cos 12\theta + \dots \end{aligned} \quad (28)$$

B. Voltage Offset

The measurement offset or the signal conversion circuits can sometimes cause voltage offset [24]. The unbalanced grid voltages can be represented by

$$\begin{aligned} v_a &= V_m \cos \theta + V_{a0} \\ v_b &= V_m \cos\left(\theta - \frac{2\pi}{3}\right) + V_{b0} \\ v_c &= V_m \cos\left(\theta + \frac{2\pi}{3}\right) + V_{c0} \end{aligned} \quad (29)$$

where V_{a0} , V_{b0} , and V_{c0} represent the offset voltage levels.

The voltages in the $\alpha\beta$ frame are as follows:

$$\begin{aligned} v_{\alpha} &= V_m \cos \theta + V_{\alpha 0} \\ v_{\beta} &= V_m \cos \theta + V_{\beta 0} \end{aligned} \quad (30)$$

where $V_{\alpha 0} = 2/3(V_{a0} + V_{b0} + V_{c0})$, and $V_{\beta 0} = 1/\sqrt{3}(V_{c0} - V_{b0})$.

The q -axis voltage can be derived and linearized by

$$\begin{aligned} v_{qe} &= V_m \sin \delta + V_{\alpha 0} \sin \hat{\theta} + V_{\beta 0} \cos \hat{\theta} \\ &\approx V_m \delta + E_{\omega} \cos(\theta + \phi_0) \end{aligned} \quad (31)$$

where

$$E_{\omega} = \sqrt{V_{\alpha 0}^2 + V_{\beta 0}^2}, \quad \phi_0 = -\tan^{-1}\left(\frac{V_{\alpha 0}}{V_{\beta 0}}\right).$$

The phase error caused by the offset has the same frequency component as that of the grid voltage [24]. The phase error caused by the voltage offset is given by

$$\delta = \frac{E_{\omega}}{V_m} \cos(\theta + \phi_0). \quad (32)$$

The total disturbances present in ESO-based PLL control system can be expressed by

$$f = [(b - b_0)\Delta\hat{\omega} + (\omega_g - \omega) + d_x] + \omega \frac{E_{\omega}}{V_m} \sin(\theta + \phi_0). \quad (33)$$

REFERENCES

- [1] J. Chen, R. J. Patton, and H.-Y. Zhang, "Design of unknown input observers and robust fault detection filters," *Int. J. Control*, vol. 63, no. 1, pp. 85–105, Jan. 1996.
- [2] W. Chen, J. Yang, L. Guo, and S. Li, "Disturbance-observer-based control and related methods—An overview," *IEEE Trans. Ind. Electron.*, vol. 63, no. 2, pp. 1083–1095, Feb. 2016.
- [3] J. Han, "From PID to active disturbance rejection control," *IEEE Trans. Ind. Electron.*, vol. 56, no. 3, pp. 900–906, Mar. 2009.
- [4] Z. Gao, "Scaling and bandwidth-parameterization based controller tuning," in *Proc. Amer. Control Conf.*, vol. 6, 2006, pp. 4989–4996.
- [5] R. Madoński and P. Herman, "Survey on methods of increasing the efficiency of extended state disturbance observers," *ISA Trans.*, vol. 56, pp. 18–27, May 2015.
- [6] Y. Huang and W. Xue, "Active disturbance rejection control: Methodology and theoretical analysis," *ISA Trans.*, vol. 53, no. 4, pp. 963–976, Jul. 2014.
- [7] B. Guo, S. Bacha, M. Alamir, A. Mohamed, and C. Boudinet, "LADRC applied to variable speed micro-hydro plants: Experimental validation," *Control Eng. Pract.*, vol. 85, pp. 290–298, Apr. 2019.
- [8] B. Guo, S. Bacha, and M. Alamir, "A review on ADRC based PMSM control designs," in *Proc. 43rd Annu. Conf. IEEE Ind. Electron. Soc. (IECON)*, Oct. 2017, pp. 1747–1753.
- [9] B.-Z. Guo and Z.-L. Zhao, "On the convergence of an extended state observer for nonlinear systems with uncertainty," *Syst. Control Lett.*, vol. 60, no. 6, pp. 420–430, Jun. 2011.
- [10] D. Yoo, S.-T. Yau, and Z. Gao, "On convergence of the linear extended state observer," in *Proc. IEEE Int. Symp. Intell. Control*, Oct. 2006, pp. 1645–1650.
- [11] Q. Zheng, L. Q. Gao, and Z. Gao, "On stability analysis of active disturbance rejection control for nonlinear time-varying plants with unknown dynamics," in *Proc. 46th IEEE Conf. Decis. Control*, Dec. 2007, pp. 3501–3506.
- [12] A. A. Godbole, J. P. Kolhe, and S. E. Talole, "Performance analysis of generalized extended state observer in tackling sinusoidal disturbances," *IEEE Trans. Control Syst. Technol.*, vol. 21, no. 6, pp. 2212–2223, Nov. 2013.
- [13] B. Sun and Z. Gao, "A DSP-based active disturbance rejection control design for a 1-kW H-bridge DC–DC power converter," *IEEE Trans. Ind. Electron.*, vol. 52, no. 5, pp. 1271–1277, Oct. 2005.
- [14] R. Miklošovic, A. Radke, and Z. Gao, "Discrete implementation and generalization of the extended state observer," in *Proc. Amer. Control Conf.*, Jun. 2006, p. 6.
- [15] J. A. Cortes-Romero, A. Luviano-Juarez, and H. Sira-Ramirez, "Robust GPI controller for trajectory tracking for induction motors," in *Proc. IEEE Int. Conf. Mechatronics*, Apr. 2009, pp. 1–6.
- [16] J. Cortés-Romero, G. A. Ramos, and H. Coral-Enriquez, "Generalized proportional integral control for periodic signals under active disturbance rejection approach," *ISA Trans.*, vol. 53, no. 6, pp. 1901–1909, Nov. 2014.
- [17] G. A. Ramos, J. Cortés-Romero, and H. Coral-Enriquez, "Spatial observer-based repetitive controller: An active disturbance rejection approach," *Control Eng. Pract.*, vol. 42, pp. 1–11, Sep. 2015.
- [18] K. K. Busawon and P. Kabore, "Disturbance attenuation using proportional integral observers," *Int. J. Control*, vol. 74, no. 6, pp. 618–627, Jan. 2001.
- [19] M. Andreica, S. Bacha, D. Roye, I. Munteanu, A. I. Bratcu, and J. Guiraud, "Cross-flow water turbines control under grid disturbances," in *Proc. IEEE Bucharest PowerTech*, Jun. 2009, pp. 1–6.
- [20] G. Wu, L. Sun, and K. Y. Lee, "Disturbance rejection control of a fuel cell power plant in a grid-connected system," *Control Eng. Pract.*, vol. 60, pp. 183–192, Mar. 2017.
- [21] R. M. S. Filho, P. F. Seixas, P. C. Cortizo, L. A. B. Torres, and A. F. Souza, "Comparison of three single-phase PLL algorithms for ups applications," *IEEE Trans. Ind. Electron.*, vol. 55, no. 8, pp. 2923–2932, Aug. 2008.
- [22] M. H. J. Bollen, "Voltage recovery after unbalanced and balanced voltage dip in three-phase systems," *IEEE Power Eng. Rev.*, vol. 22, no. 10, pp. 63–64, Oct. 2002.
- [23] I. Etxeberria-Otadui, A. L. De Heredia, H. Gaztanaga, S. Bacha, and M. R. Reyer, "A single synchronous frame hybrid (SSFH) multifrequency controller for power active filters," *IEEE Trans. Ind. Electron.*, vol. 53, no. 5, pp. 1640–1648, Oct. 2006.
- [24] S.-K. Chung, "A phase tracking system for three phase utility interface inverters," *IEEE Trans. Power Electron.*, vol. 15, no. 3, pp. 431–438, May 2000.

- [25] H. Bevrani, A. Ghosh, and G. Ledwich, "Renewable energy sources and frequency regulation: Survey and new perspectives," *IET Renew. Power Gener.*, vol. 4, no. 5, pp. 438–457, Sep. 2010.
- [26] M. Tsili and S. Papathanassiou, "A review of grid code technical requirements for wind farms," *IET Renew. Power Gener.*, vol. 3, no. 3, pp. 308–332, Sep. 2009.
- [27] S. Golestan, J. M. Guerrero, and J. C. Vasquez, "Three-phase PLLs: A review of recent advances," *IEEE Trans. Power Electron.*, vol. 32, no. 3, pp. 1894–1907, Mar. 2017.
- [28] B. Guo, S. Bacha, M. Alamir, C. Boudinet, and H. Mesnage, "An enhanced phase-locked loop with extended state observer," in *Proc. 20th Int. Symp. Power Electron. (Ee)*, Oct. 2019, pp. 1–6.
- [29] P. Rodriguez, J. Pou, J. Bergas, J. I. Candela, R. P. Burgos, and D. Boroyevich, "Decoupled double synchronous reference frame PLL for power converters control," *IEEE Trans. Power Electron.*, vol. 22, no. 2, pp. 584–592, Mar. 2007.
- [30] S. Golestan, M. Ramezani, J. M. Guerrero, F. D. Freijedo, and M. Monfared, "Moving average filter based phase-locked loops: Performance analysis and design guidelines," *IEEE Trans. Power Electron.*, vol. 29, no. 6, pp. 2750–2763, Jun. 2014.
- [31] Z. Xin, R. Zhao, P. Mattavelli, P. C. Loh, and F. Blaabjerg, "Re-investigation of generalized integrator based filters from a first-order-system perspective," *IEEE Access*, vol. 4, pp. 7131–7144, 2016.
- [32] D. N. Zmood and D. G. Holmes, "Stationary frame current regulation of PWM inverters with zero steady state error," in *Proc. 30th Annu. IEEE Power Electron. Spec. Conf. Rec.*, Jul. 1999, pp. 1185–1190.
- [33] B. Guo, S. Bacha, M. Alamir, and H. Iman-Eini, "A robust LESO-based DC-link voltage controller for variable speed hydro-electric plants," in *Proc. IEEE Int. Conf. Ind. Technol. (ICIT)*, Feb. 2019, pp. 361–366.
- [34] J. Tatsumi and Z. Gao, "On the enhanced ADRC design with a low observer bandwidth," in *Proc. 32nd Chin. Control Conf.*, Jul. 2013, pp. 297–302.
- [35] G. Tian and Z. Gao, "Frequency response analysis of active disturbance rejection based control system," in *Proc. IEEE 22nd Int. Symp. Intell. Control*, Oct. 2007, pp. 1595–1599.
- [36] S. Zhong and Y. Huang, "Comparison of the phase margins of different ADRC designs," in *Proc. Chin. Control Conf. (CCC)*, Jul. 2019, pp. 1280–1285.
- [37] H. Jin, J. Song, S. Zeng, and W. Lan, "Linear active disturbance rejection control tuning approach guarantees stability margin," in *Proc. 15th Int. Conf. Control, Autom., Robot. Vis. (ICARCV)*, Nov. 2018, pp. 1132–1136.



Baoling Guo received the B.S and M.S. degrees from the China University of Petroleum, Qingdao, China, in 2012 and 2014, respectively, the M.S. degree from the Grenoble Institute of Technology (Grenoble INP), Grenoble, France, in 2015, and the Ph.D. degree from the Grenoble Electrical Engineering Laboratory (G2Elab), Université Grenoble Alpes, Grenoble, in 2019.

She is currently a Post-Doctoral Researcher at G2Elab. Her main research interests include variable speed hydropower generation, power electronics system modeling and control, and renewable energy integration.



Seddik Bacha (Senior Member, IEEE) received the B.S. and M.S. degrees from the École Nationale Polytechnique d'Alger, Algiers, Algeria, in 1982 and 1990, respectively, and the Ph.D. degree from the Grenoble Institute of Technology (Grenoble INP), Grenoble, France, in 1993.

In 1990, he joined the Laboratoire d'Electrotechnique de Grenoble, Grenoble. From 2001 to 2012, he was the Manager of the Power Systems Group, Grenoble Electrical Engineering Laboratory (G2Elab), Grenoble INP.

He is currently a Professor with Université Grenoble Alpes, Grenoble. His research interests include power electronics system modeling and control, power quality, and renewable energy integration.



Mazen Alamir (Member, IEEE) graduated in mechanics in Grenoble, France, in 1990, and in aeronautics in Toulouse, France, in 1992. He received the Ph.D. degree in nonlinear model predictive control from the Grenoble Institute of Technology (Grenoble INP), Grenoble, France, in 1995.

He has served as the Head of the Systems and Complexity Research Group, Control Systems Department, Gipsa-Lab, Grenoble. Since 1996, he has been a CNRS Research Associate with the Control Systems Department, Gipsa-Lab. His main

research topics are model predictive control, receding horizon observers, nonlinear hybrid systems, signature-based diagnosis, optimal cancer treatment, and industrial applications.

Dr. Alamir is also an Associate Editor of the IEEE TRANSACTIONS ON AUTOMATIC CONTROL (IEEE-TAC). His home page is www.mazenalamir.fr.



Ahmad Hably (Member, IEEE) received the B.S. degree in electrical engineering from the Lebanese University, Beirut, Lebanon, in 2004, and the M.S. degree and the Ph.D. degree in automatic control from the Grenoble Institute of Technology, Grenoble, France, in 2005 and 2007, respectively.

After one year as a Researcher [Attaché Temporaire d'Enseignement et de Recherche (ATER)] with the LIRMM Laboratory, Montpellier, France, he joined the Université Grenoble Alpes, Grenoble, as an Associate Professor with the Grenoble Image

Parole Signal Automatique Laboratory (GIPSA-Lab), Automatic Control Department. His research interests include electrical vehicle integration, nonlinear control, predictive control for energy systems, and airborne wind-energy systems.



Cédric Boudinet was born in 1981. He graduated as an Engineer in energetic engineering from the National Institute of Applied Sciences of Rouen, Saint-Étienne-du-Rouvray, France, in 2004.

From 2004 to 2010, he worked as a consultant in software development for automotive, nuclear, and electrical grid industries. Since 2010, he has been an Engineer with the Grenoble Electrical Engineering Laboratory (G2Elab), Grenoble, France. He focuses on real-time hardware and software systems.